Neurological mechanism of sensory deficits after exposure to non-dioxin-like polychlorinated biphenyls (PCBs) in zebrafish larvae

Nadja R. Brun[1], Jennifer M. Panlilio[1], Kun Zhang[2,3], Yanbin Zhao[2,3], Evgeny Ivashkin[4,5], John J. Stegeman[1], Jared V. Goldstone[1]

[1] Department of Biology, Woods Hole Oceanographic Institution, Woods Hole, MA, USA
[2] School of Environmental Science and Engineering, Shanghai Jiao Tong University, 800 Dongchuan Road, Shanghai 200240, China
[3] Shanghai Institute of Pollution Control and Ecological Security, Shanghai 200092, China
[4] Josephine Bay Paul Center for Comparative Molecular Biology and Evolution, Marine Biological Laboratory, Woods Hole, MA, USA
[5] A.N. Severtsov Institute of Ecology and Evolution, Russian Academy of Sciences, Moscow, Russia

Address correspondence to
Nadja Brun, nbrun@whoi.edu

Woods Hole Oceanographic Institution, Mail Stop 32
266 Woods Hole Road
Woods Hole, MA 02543

Competing Financial Interests

The authors declare they have no actual or potential competing financial interests.

Abstract

Background: The most abundant polychlorinated biphenyl (PCB) congeners found in the environment and in humans are the *ortho*-substituted, non-dioxin-like (NDL) congeners, especially PCB153. While evidence indicates that exposure to PCB153 and other NDL-PCBs in early vertebrate development can contribute to neurobehavioral disorders, the basis of neurobiological effects of NDL-PCBs is poorly understood.

Methods: We assessed a range of effects of several NDL-PCB congeners (PCB153, PCB52, PCB118, and PCB138) on cellular morphologies and synaptic transmission linked to the proper execution of a sensorimotor response in zebrafish, taking advantage of the well-established neural circuit in this model. Specifically, we imaged hair cells, neurons, and muscle tissue to evaluate their presence and morphology. We measured neurotransmitter levels in larvae and assessed the mechanosensory startle response in co-exposures to PCB153 and neurotransmitter modulators to evaluate the involvement of neurotransmitters in the behavioral response. The startle response was also assessed in dioxin-like (DL)-PCB126 exposed larvae.

Results: Startle responses were dramatically delayed in 6-day old larvae exposed to NDL-PCB. In contrast, exposure to the DL PCB126 did not delay startle response times. Morphological and biochemical data showed that exposure to NDL-PCBs during development induces swelling of afferent sensory neurons and disrupts dopaminergic and GABAergic signaling associated with motor movement.

Discussion: This study demonstrates that connections between neurotoxic mechanisms and processing of sensory stimuli occur at low concentrations of NDL-PCBs, similar to those present in human and animal samples. The effects on important and broadly conserved signaling mechanisms in vertebrates suggest that NDL-PCBs can contribute to neurodevelopmental abnormalities, relevant for both exposed human populations and wildlife.

Introduction

Humans and wildlife are exposed to a wide range of contaminants in the environment, and the role of these chemical pollutants in developmental neurotoxicity, cognitive impairment, and neurodegenerative disorders has become a global environmental health concern (Landrigan et al. 2018). Among the top industrial chemicals thought to be involved in developmental neurotoxicity are polychlorinated biphenyls (PCBs) (Grandjean and Landrigan 2014), a mix of 209 different structures, including planar dioxin-like (DL) congeners and non-planar non-dioxin-like (NDL) congeners. PCBs are persistent legacy contaminants that have been produced and used for decades to serve as insulators, coatings, and caulks, and there is worldwide PCB contamination of wildlife tissue and human cord blood, amniotic fluid, and mother's milk (Ennaceur et al. 2008; Lancz et al. 2015a). The developing nervous system is generally sensitive to chemical exposure at doses much lower than those affecting adult nervous system function (Rice and Barone 2000). For instance, prenatal exposure to PCBs is associated with a decrease in motor skills in infants, while postnatal exposure seems to have no obvious effects (Ribas-Fitó et al. 2001). Thus, identifying the mechanisms underpinning the effects of neurotoxic PCBs during gestation and early life stages is of critical importance in attaining successful treatments and remediating health effects in humans and wildlife due to environmental exposure.

The NDL-PCBs are the most abundant congeners in human and environmental samples. The NDL-PCB138 and PCB153, are particularly abundant. Median PCB153 concentrations measured in human cord blood serum range from 6.4 to 110 ng g^{-1} lipid (Bergonzi et al. 2009; Herbstman et al. 2007; Lancz et al. 2015b), far greater than the levels of DL congeners. Evidence also suggests the NDL-PCBs contribute substantially to neurotoxic and behavioral effects (Boix et al. 2010; Boucher et al. 2009). However, understanding of the mechanisms and effects of NDL-PCBs, especially during the more sensitive early stages of development, significantly lags that of DL-PCBs.

Increased serum PCB concentrations in children are associated with deficits in cochlear functions (Jusko et al. 2014; Trnovec et al. 2010), fine motor skills (Walkowiak et al. 2001), and cognitive impairment (Boucher et al. 2009; Chen et al. 1992). Developmental exposure of rats to NDL-PCBs has been linked to behavioral changes, including hyperactivity, impulsiveness, and impairment of cognitive function (e.g., impairment of the ability to learn the Y maze task) (Berger et al. 2001; Boix et al. 2010; Johansen et al. 2014). NDL-PCB developmental exposure also adversely affects auditory function in adult rats, including elevated thresholds of brainstem auditory evoked potentials, auditory deficits at low frequencies, audiogenic seizures, and reduced auditory startle responses (Crofton et al. 2000; Goldey et al. 1995; Lilienthal et al. 2011, 2015; Poon et al. 2015). The mechanism(s) involved in these effects on cognitive and auditory systems are not known.

Zebrafish are increasingly used as model organism to uncover the mechanisms of neurotoxicity that are relevant for humans and other vertebrates. Zebrafish remain transparent throughout early development, facilitating the use of transgenic and other molecular approaches to label and observe specific classes of neurons and to follow their functional development. Fish have relatively simple neural circuits, particularly for the auditory system. In fish, the auditory-evoked startle response plays a critical role in animal survival, and involves cellular functions, sensory-motor pathways, and monoamine neurotransmitters that are conserved among vertebrates (Stewart et al. 2014). Many of the pathways and genes that regulate zebrafish startle behavior also operate in human neurological disorders (Howe et al. 2013; Maximino and Herculano 2010; Meserve et al. 2020; Tropepe and Sive 2003; Wolman et al. 2015). In this study, we use the zebrafish startle response to decipher the neuro-disruptive basis of NDL-PCBs on the auditory system during the early stages of development. To this end, we examined the effects of different NDL-PCBs (PCB153, PCB52, PCB118, PCB138), in comparison to the DL-PCB126 and at different environmentally relevant concentrations, dissecting various steps in the neural circuitry underlying the acoustic startle response.

Materials and Methods

Animal model

In addition to other attributes, zebrafish have relatively simple neural circuits, particularly for the auditory system. Many of the components of the auditory circuit are homologous in mammals and fish, including hair cells, neural transmission, and lower motorneurons, while the mechanosensory lateral line system and Mauthner (M) cells are exclusively found in fish and a cochlea is only found in mammals. In fish, vibro-acoustic stimuli are first sensed by the hair cell bundles in the auditory, vestibular, and lateral-line systems and rapidly encoded into trains of action potentials in the afferent neurons (**Figure 1**) (Hudspeth 1985). The signal detected through the sensory hair cells of the lateral line is transmitted through the anterior and posterior lateral line ganglia whereas the auditory input is transmitted through the VIIIth statoacoustic nerve, all of which synapse to the lateral dendrite of the M-cell and two segmental homologs (Nakayama 2004; Pujol-Martí and López-Schier 2013). The signal is propagated down the M-cell axon in the spinal cord to activate the motoneurons leading to a unilateral contraction of the trunk musculature.

Zebrafish husbandry and early-life stage exposure

Zebrafish (*Danio rerio*) were maintained at 28.5 °C and on a 12:12 h light-dark cycle according to the guidelines of the Zebrafish Model Organism Database (ZFIN, http://zfin.org) and institutional guidelines at WHOI and the experimental procedures approved by the Institutional Animal Care and Use Committee (ID Number BI21981.01). Adult zebrafish were fed brine shrimp and pellets every day. In this study, we used wild-type zebrafish of the AB strain obtained from Zebrafish International Resource Center (ZIRC), as well as several transgenic lines: the photoconvertible calcium indicator line *Tg[elavl3:CaMPARI(W391F+V398L)]*^{jf9} kindly provided by Jessica Plavicki (Brown University, USA), and the transgenic lines *Tg(cntn1b:EGFP-CAAX)* (Panlilio et al. 2021) labeling axons, *Tg(olig2:EGFP)*^{vu12} (Park et al. 2007; Shin et al. 2003) marking oligodendrocyte precursor cell bodies, *Tg(sox10:mRFP)* (Takada et al. 2010) marking oligodendrocyte lineage cells, as

well as *Tg(mbp:EGFP-CAAX)* (Almeida et al. 2011) *and Tg(mbp:EGFP)* (gift from Dr. Kelly Monk, generated by Dr. Charles Kaufman in the laboratory of Dr. Leonard Zon, Harvard Medical School, Boston, MA) marking myelin sheaths. Zebrafish eggs were obtained by pairwise breeding and kept in 0.3x Danieau's (17 mM NaCl, 0.2 mM KCl, 0.12 mM $MgSO_4$, 0.18 mM $Ca(NO_3)_2$ and 1.5 mM HEPES, pH 7.6) in glass vials at a density of 10 individuals per 10 mL, at a constant water temperature of 28 ± 1˚C and standard 14-h light/10-h dark cycle. The medium was supplemented with 1-Phenyl-2-thiourea (PTU, 0.003% w/v) from 24 hours post-fertilization (hpf) onwards to prevent pigment formation when necessary for imaging. Fertilized eggs were used for exposures starting at 3 hpf to solvent control (0.1% DMSO, v/v), 2,2′,4,4′,5,5′-hexachlorobiphenyl (PCB153), 2,2′,5,5′-PCB, 2,2′,5,5′-tetrachlorobiphenyl (PCB52), 2,3',4,4',5-pentachlorobiphenyl (PCB118), 2,2',3,4,4',5'-hexachlorobiphenyl (PCB138), or 3,3',4,4',5-hexachlorobiphenyl (PCB126). Additionally, one exposure scenario with PCB153 was started at 24 hpf, to assess whether effects are induced during or after initial neuronal cell differentiation. Sensory neurons send their projection along the ectoderm as early as 16 hpf (Kimmel 1993). The lowest exposure concentration for PCB153 was 10 nM (3.6 ng mL^{-1}) which is estimated to result in ~5 ng g^{-1} (5 ppm) per zebrafish larvae (comparing to PCB95 uptake levels; (Ranasinghe et al. 2019)). PCB153 mean concentrations found in maternal cord blood serum are 0.27 ng mL^{-1} or 110 ng g^{-1} lipid (Lancz et al. 2015b)). Other concentrations used were 30, 100, and 1000 nM which are found in fish of contaminated ecosystems (Gräns et al. 2015). For PCB52, PCB118, and PCB138, a concentration of 1000 nM was chosen to compare to the highest effect concentration of PCB153. The DL-PCB126 is cardioteratogenic in the low nanomolar range. To avoid malformations, a concentration of 1 nM was chosen. Exposures were refreshed daily until four days post-fertilization (dpf) and all larvae were kept in Danieau's from 5 to 6 dpf. All imaging and behavioral assays were performed at 6 dpf, except for the touch assay, which was performed at 26 hpf.

The influence of neurotransmitters on the startle behavior was assessed by exposures to compounds known to interfere with monoamines. At 6 dpf, larvae were evaluated for their startle behavior and then immersed in the dopamine precursors L-DOPA (1 mM) or L-tyrosine (1 mM), dopamine receptor agonist quinpirole (10 µM), dopamine D2-receptor antagonist and GABA receptor modulator haloperidol (10 µM), endogenous serotonin 5-HT (10 µM), and serotonin precursor 5-HTP (1 mM) for 30 min in the well plate before assessing the startle behavior again. Additionally, the effect of neurotransmitter modulation during development on startle response was assessed by exposing larvae from 3 to 120 hpf to L-DOPA (1 mM), L-tyrosine (1 mM), and quinpirole (10 µM).

Behavioral Analysis

Larval locomotion was monitored using the Noldus Daniovison system (Noldus Information Technology, Leesburg, VA, USA) using 6-dpf larvae distributed in 48-well plates (1 larva per well). After an acclimation period of 40 minutes in the illuminated chamber, spontaneous swimming activity was tracked for 10 minutes. Following the spontaneous swimming, three alternating cycles of dark and light conditions (10 minutes each) were run. The experiment was repeated three times with cohorts from separate breeding events (n = 24 per group and breeding event). Video data were recorded with 30 frames per second via an infrared camera. Obtained data were analyzed with the supplied software EthoVision XT® 12 (Noldus. Inc.).

The activity of Rohon-Beard sensory neurons was tested at 26 hpf by lightly touching DMSO- and 1000 nM PCB153-exposed embryos (n = 10 per group and breeding event) using a piece of fishing line affixed to a glass pipette. Each embryo was touched ten times and the response was scored as follows: 0, no response; 0.5, light tail flicking response, 1, coiling in the opposite direction of the touch stimulus, yielding a score of maximum 10 per embryo. The experiment was repeated twice with cohorts from separate breeding events.

Vibro-acoustic startle response was assessed as described previously (Panlilio et al. 2021). Briefly, the acoustic stimuli were delivered by a vibrational exciter producing acoustic vibrations at a frequency of a 1000 Hz for a duration of 2 ms at four different amplitudes (32, 38, 41, 43 dB). For each amplitude, the stimulus was delivered four times, spaced 20 seconds apart, to a 4 x 4 well-plate mounted on top of the speaker, each well containing an individual larva. The response was tracked with a high-speed camera (Edgertronic SC1) at 1000 frames s^{-1} for 250 ms (13 ms before and 237 ms after the stimulus). PulsePal was used to synchronize the camera recording to the acoustic stimuli using a TTL pulse. Automated analysis of larval movement kinematics (response frequency, latency, turning angle) was performed using the FLOTE software package (Burgess and Granato 2007). Each treatment group was assessed at least three times with eggs from different clutches. The total replicate numbers are stated in the **Table S1 (Supplemental Material)**.

A startle response in fish can be executed with a short latency C-bend (SLC) or long latency C-bend (LLC), with the SLC being the more frequent response at higher stimulus intensities. The cut-off time between SLC and LLC can vary depending on environmental conditions such as temperature and has been determined empirically for this experiment using a Gaussian mixture model (Panlilio et al. 2020)(**Figure S1**). Responses within 15 ms were categorized as SLC, latencies greater than 15 ms as LLC. Following this classification, the median response type (Relative Startle Bias) for each responsive fish was determined for each stimulus intensity (32, 38, 41, and 43 dB). Bias per individual fish was calculated as: (frequency of SLC – frequency of LLC) / total responses. Pure SLC responses result in a value of +1, while pure LLC responses are a value of -1 (Jain et al. 2018).

Electric field pulses (EFPs) directly activate the M-cells (Tabor et al. 2014). Responsiveness of M-cells was assessed by applying EFPs (4.4 V cm^{-1} for 2 ms, square pulse) to head-restrained larvae (n = 46 per treatment group). Seven consecutive EFPs were applied with a recovery time of 20 s in between pulses. For each run, one control and one exposed larva were embedded in 1.5% agarose side-by-side and their tails freed. Response frequency,

206 latency, and bend angle were tracked using FLOTE. For all behavioral assays, only larvae
207 with an inflated swim bladder were used.

208 **Larval growth**

209 Larval length (from snout to the tail-fin end) was measured in DMSO (*n* = 57) and 1000 nM
210 PCB153 (*n* = 51) exposed larvae using ImageJ. The experiment was performed three times
211 with embryos from different clutches.

212 **FM1-43 labeling in hair cells**

213 The vital fluorescent dye FM1-43 (n-(3-triethylammoniumpropyl)-4-(4-(dibutylamino)-styryl)
214 pyridinium dibromide; Invitrogen) specifically labels hair cells in the lateral line and inner ear
215 of vertebrates of by entering through open mechanotransduction channels and filling the
216 cytoplasm of hair cells (Meyers et al. 2003). At 6 dpf, zebrafish larvae of 1000 nM PCB153-
217 exposed (*n* = 32) and unexposed (*n* = 28) groups were immersed in Danieau's
218 supplemented with 3 µM FM1-43 for 30 s, rinsed three times in Danieau's, anesthetized in 1
219 mM 3-amino-benzoic acid (Tricaine), and mounted in 1.5% low melting agarose for confocal
220 imaging of the L3 neuromast. The experiment was performed three times independently.

221 **Immunohistochemistry to stain M-cells, kinocilia, and muscle fibers**

222 Whole-mount immunohistochemistry of zebrafish larvae and brains was performed following
223 standard procedures. Briefly, 10 AB larvae per exposure group were treated as described
224 above and subsequently fixed in 4% paraformaldehyde (PFA) in PBS overnight at 4 ˚C. For
225 labelling brain tissue, larval brains were dissected before continuing with the protocol.
226 Multiple rinsing steps in PBS containing either 0.5% Triton-X100 or 0.1% Tween-20 (PBST)
227 for larvae or brains, respectively, was followed by an antigen retrieval step in 150 mM Tris
228 HCl (pH 9.0) at 70 °C (Inoue and Wittbrodt 2011), and a permeabilization step using
229 proteinase K (10 µg/mL for 3 minutes). Subsequently, the samples were blocked in blocking
230 solution (10% Normal Goat Serum, 1% DMSO, 1% BSA, 88% PBST) for 1 h and then
231 stained with blocking solution supplemented with the primary antibody for three days at 4 ˚C.

The primary anti-neurofilament mouse polyclonal antibody (3A10; Developmental Hybridoma Bank, 1:100 dilution) was used to label a subset of hindbrain spinal cord projecting neurons such as the M-cell neurons (DMSO *n* = 23, PCB153 *n* = 21). The anti-5HT rabbit polyclonal antibody (Sigma-Aldrich, #S5545, 1:500) was used to label serotonergic cells (DMSO *n* = 16, PCB153 *n* = 13). The anti-acetylated alpha-tubulin mouse polyclonal antibody (Sigma-Aldrich, #T6793, 1:1000 dilution) was used to label kinocilia and hair cell innervating neurons (DMSO *n* = 25, PCB153 *n* = 24). After several washing steps, in PBST, the samples were incubated with Alexa Fluor 488- or 594-conjugated goat-anti-mouse or goat-anti-rabbit secondary antibodies (Abcam, 1:500 dilution) overnight at 4 ˚C and rinsed several times in PBST before mounting in ProLong Diamond Antifade mountant (Invitrogen) for imaging. For visualization of skeletal muscle fibers (DMSO *n* = 11, PCB153 *n* = 11), larvae were fixed as above, followed by permeabilization in 5% Triton-X for overnight and incubation in phalloidin Alexa-546 conjugate (Invitrogen, 1:500). All staining experiments were repeated three times with larvae from independent clutches except the phalloidin staining, which were performed once.

Imaging of hair cell innervating neurons, primary motoneuron, and oligodendrocyte lineage cells

The *Tg(cntn1b:EGFP-CAAX)* transgenic line was used to image the cell bodies of neurons that innervate the hair cells at the L3 position in the lateral line (DMSO *n* = 22, PCB153 *n* = 20, two independent experiments). The axons of the main caudal primary motoneurons were visualized using the *Tg(olig2:EGFP)* transgenic line (*n* = 4 per treatment group, one experiment). The double transgenic *Tg(olig2:EGFP) x Tg(sox10:mRFP)* was used to quantify oligodendrocyte lineage cells in the spinal cord of in DMSO (*n* = 22) and 1000 nM PCB153 (*n* = 16) treated larvae (Shin et al. 2003). All larvae were anesthetized in tricaine (0.16% MS222) before mounting laterally in 1.5% low melting agarose on a glass-bottom microscopy dish (MatTek). Fluorescently-labeled cell bodies were imaged at the distal end of the

intestine, around the L3 neuromast. The experiments were performed three times independently.

Calcium imaging of freely swimming and startling larvae

Neuronal activity in DMSO- and PCB153-treated larvae was visualized using the CaMPARI (*elavl3*:CaMPARI) transgenic zebrafish line with an engineered fluorescent protein that permanently photoconverts from green to red in the presence of elevated calcium and UV light (Fosque et al. 2015). Photoconversion was achieved by mounting an LED light (405 nm; LEDSupply) between the speaker and a custom-made 3-well plate containing the freely swimming larvae (DMSO- and PCB153-treated). Larvae of the same treatment were divided into two batches: one was photoconverted in medium at room temperature (RT) and the other one at 4˚C to elicit high neuronal activity. Photoconversion was achieved by shining the LED light for 10 sec either with one vibrational stimulus of 43 dB at the start or without stimulus. Subsequently, larvae were anesthetized, embedded in agarose, and whole brains imaged using the 10x objective. The experiment was performed twice (n = 11-16 per treatment group).

Image processing

Whole-brain, hair cells, M-cell, and motor neurons were imaged on a Zeiss LSM 800 confocal system with a 10x/0.45 Plan-Apochromat, 20x/0.8 Plan-Apochromat, or 63x/1.2 C-Apochromat water immersion objective. Airy scan was applied for hair cell imaging at 63x. Z-stacks were merged to a single plane by maximal intensity projection using Fiji (Schindelin et al. 2012). The number of *olig2* cells dorsal of the spinal cord (DMSO n = 22, 1000 nM PCB153 n = 16) was counted in confocal image stacks using the 3D projection of the Zeiss Zen blue software. Myelination was evaluated after imaging the spinal cord (DMSO n = 26, 1000 nM PCB153 n = 27) using the 20x objective and scored for deficits according to Panlilio et al. 2020. Representative myelination was imaged at 40x. The intensity of serotonergic neurons in the brain (DMSO n = 16, 1000 nM PCB153 n = 13) was measured performing a

Sum Slices Z-projection followed by drawing a ROI around the 5-HT immuno-responsive cells, and per image, three random squares (area size = 10.65 x 10.65) within the non-fluorescent area of the ROI for background subtraction (for orientation see **Figure S12**). Similarly, the FM1-43 intensity was measured drawing a ROI around the fluorescent hair cells and measuring the background in three random squares (DMSO *n* = 20, 1000 nM PCB153 *n* = 20). Corrected total cell fluorescence (CTCF) was calculated according to the formula: Integrated density - (ROI x Mean fluorescence of background readings). For quantification of active neurons in the brain of freely swimming and startling CaMPARI zebrafish larvae, Sum Slices Z-projection were analyzed for red fluorescence intensity in the rostral hindbrain (for orientation see **Figure S13**).

The volume of hair cell innervating neurons was calculated by measuring the volume of threshold pixels (30-255, Otsu method) in image stacks using an imageJ macro looping through the stack and summing the area measurements, then multiplying this sum by the depth of each slice (DMSO *n* = 30, 1000 nM PCB153 *n* = 29). The presence of primary motor neurons was confirmed using the Simple Neurite Tracer plugin in Fiji (DMSO *n* = 21, 1000 nM PCB153 *n* = 18). All image evaluations and quantifications were done without the knowledge of the experimental condition of the specimens.

Neurotransmitter analysis

The analysis of neurotransmitters, including histamine, L-histidine, L-glutamic acid, gamma-aminobutyric acid (GABA), acetylcholine, L-DOPA, 3-methoxytyramine, serotonin, 5-hydroxyindole-3-acetic acid, glycine, L-glutamine, L-valine, 3-hydroxytyramine and choline, was performed with a method developed in a previous study (Zhao et al. 2020). Briefly, the zebrafish embryo samples were spiked with 100 ppb isotope-labeled internal standards and then homogenized. The homogenized tissue samples were extracted with 200 µL of 80:20 v/v ACN/Milli-Q water containing 0.1% formic acid and 1% ascorbic acid and 200 µL ACN. After protein precipitation, the supernatants were dried and redissolved in 100 µL of Milli-Q water containing 0.1% formic acid for UHPLC-MS/MS analysis. Neurotransmitters were

quantified by a high-performance liquid chromatography system coupled to a Q-Exactive plus quadrupole-Orbitrap mass spectrometer (UHPLC-Q-Orbitrap, Thermo fisher, US). The separation of neurotransmitters was carried out with an Acquity UPLC HSS T3 column with Milli-Q water containing 0.1% formic acid and ACN containing 0.1% formic acid as mobile phase. The MS acquisition was performed in the full scan mode and parallel reaction monitoring mode. The experiment was performed once (n = 4 per treatment group).

Statistical Analyses

All statistical analyses were conducted using Graph Pad Prism 8.4 except some of the startle behavior analysis, which was completed in R. All quantitative data were tested for normality using the Shapiro-Wilk test, and if there were unequal number of subjects between groups, the data were tested for homogeneity in variances using the Brown-Forsythe test. All treatment groups were compared to respective control groups.

Responsiveness to auditory stimuli (response or not) and startle type (SLC vs. LLC) was modeled in R (version 4.0.2) using a binomial generalized linear mixed effect model (glmer() from the lme4 R package) (Bates et al. 2015). The response to electrical stimulus was modeled using glm() from the lme4 R package. For the auditory response, we included treatment as a fixed effect and the replicate experimental trials as a random effect. The model specification for “fraction responding” was as follows: Responders ~ TreatmentGroup + (TreatmentGroup|trial). The model specification for “startle bias” was as follows: SLCorLLCresponse ~ TreatmentGroup + stimdB + (1|trial). The data were analyzed fitting the model for each stimulus intensity independently. The model specification for the electrical stimulation are as follows: Responders ~ TreatmentGroup.

To assess treatment differences of normal data with three or more groups (fluorescence intensity CaMPARI), ANOVA comparisons were performed followed by a multiple comparison using the Tukey’s correction to adjust the critical values. A Tukey-corrected p-value < .05 was considered statistically significant. For normal data with heterogeneity

337 within-group variances (LLC bend angle), a Welch ANOVA followed by a Dunnett's T3
338 multiple comparison test was performed. For non-normal data with three or more groups
339 (SLC bend angle), a Kruskal-Wallis followed by the Dunn's multiple comparison test was
340 performed. For normal data with two groups (length, mean latency, bend angle in e-stim,
341 oligodendrocyte lineage cell count, 5-HT intensity), an unpaired two-tailed t-test with Welch's
342 correction (Welch's t- test) was performed. The nonparametric scoring data of the touch
343 assay and latency in e-stim was analyzed using a two-tailed Mann-Whitney test. The data
344 are presented as mean ± *SD* with single data points (replicates) superimposed on the graph
345 unless specified in the figure legend.

346 # Results

347 The startle response circuit is of wide relevance and well-established for assessing the
348 influence of specific factors on neuronal cell development, neuromuscular connectivity, and
349 transmission (Burgess and Granato 2007; Medan and Preuss 2014; Meserve et al. 2020;
350 Panlilio et al. 2020). We used the startle response circuit to assess the effects of NDL-PCBs
351 on the formation of neuronal populations and neurotransmission and its consequences for
352 mechanosensory disruptions, thus encompassing hearing and touch.

353 **Behavioral effects**

354 Rohon-Beard cells are the earliest mechanosensory neurons that develop. They are located
355 in the dorsal region of the embryonic spinal cord and appear around 24 hpf (Roberts 2000).
356 A few days into development, Rohon-Beard cells also relay sensory information to the M-
357 cells (Liu and Hale 2017). In our experiments, a tactile stimulus on the trunk at 26 hpf evoked
358 a C-shaped body flexion in both the DMSO- and the 1000 nM PCB153-treated embryos (U =
359 183, p = .599; **Figure S2**), indicating that the formation and function of Rohon-Beard cells
360 were not impaired by PCB153.

Exposure to contaminants during development can result in reduced growth, which can affect kinematics in swimming behavior (Voesenek et al. 2018). PCB153-exposed larvae developed normally with no difference in body length on day six in comparison to the control group, in all three trials (Trial 1: $t(25.98) = .661$, $p = .514$; Trial 2: $t(37.98) = .443$, $p = .660$; Trial 3: $t(37.43) = .645$, $p = .523$; **Figure S3**). At 6 dpf, spontaneous and light-dark-stimulated swimming activity was assessed. Larvae exposed to PCB 153 (1000 nM) had lower cumulative locomotion activity over ten minutes ($M = 1182$ mm, $SD = 382$) in comparison to the control group ($M = 1510$ mm, $SD = 402$), $t(132.4) = 4.854$, $p < .0001$ (**Figure S4A**). Zebrafish larvae typically increase locomotion in dark conditions following light exposure. Once stimulated with a rapid loss of illumination during the dark phase, both treatment groups exhibited similar swimming activity (**Figure S4B**).

The vibro-acoustic startle response can be executed either rapidly, within 15 ms (short latency C-bend; SLC), or beginning at longer times and extending for up to 100 ms (long latency C-bend; LLC). The mean latency value, representing the population response including SLC and LLC responses, was 21 ± 20 ms for control larvae at the highest stimulus intensity (**Figure S1**, **Figure 2A, B**). By contrast, the NDL-PCB-treated larvae that responded to the vibro-acoustic stimulus showed significantly longer average latencies in response to the same auditory stimulus given the controls, $F(5, 907 = 14.61$, $p < .0001)$. PCB153-treated (1000 nM) larvae responded at a mean latency of 68 ± 32 ms, PCB138 at 52 ± 37 ms, PCB118 at 45 ± 27 ms, and PCB52 at 39 ± 32 ms. For PCB153, a dose-dependent response was observed, with mean latencies increasing with dose (10 nM: 26 ± 27 ms, 30 nM: 50 ± 36 ms, 100 nM: 50 ± 30 ms, 1000 nM: 68 ± 32 ms). The lowest PCB153 concentration tested (10 nM) was not significantly different from controls. Unlike NDL-PCB treated larvae, the DL-PCB126-treated larvae had a mean latency (22 ± 22 ms), which was not significantly different from controls.

Examining the SLC and LLC responses separately can give insight into the underlying mechanism of effect. A greater stimulus intensity increases the probability of evoking SLC,

shifting the response bias from LLC to SLC (Troconis et al. 2017). Here, we also observed a shift to SLC with increasing stimulus intensity in solvent control (DMSO-treated) larvae (**Figure 2C, Figure S5A**). Larvae were tested four times at each stimulus intensity; thus, a larva is categorized as having SLC bias if it responded 3 or 4 times out of 4 stimuli with an SLC. At the highest stimulus intensity that we tested (43 dB), the majority of control larvae (300/448) responded with a SLC within 7 ± 3 ms. 43 larvae showed no bias towards SLC or LLC (2 times SLC and 2 times LLC, bias = 0). Those that did not perform an SLC (n = 105) exhibited an LLC with a mean latency of 54 ± 29 ms (**Figure 2C**). In contrast, all NDL-PCB-treated larvae (except for 10 nM PCB153) retained a response bias towards LLC at all stimulus intensities tested, which was significantly different from the control (p < .001 for all stimulus intensities). Lowering the PCB153 dose gradually increased the shift towards SLC, yet 10 nM PCB153 was still significantly different from the control (p <.01 for all stimulus intensities). Exposures starting after many structures of the brain and the neural tube have developed, at 24 hpf (Smith and Kimelman 2019), had the same effect on startle latency (**Figure S5B)**.

The proportion of control larvae responding to the stimulus (either SLC or LLC) increased from 75.2 ± 33.0% (n = 450) to 95.8 ± 17.0% (n = 457) from the lowest to highest stimulus intensity, whereas the proportion of NDL-PCB153-, PCB138-, and PCB52-treated larvae that responded remained below 70% (except for 10 nM PCB153) at all intensities and were significantly different (p < .01) from the control (**Figure 2D**, **Figure S6A**). In contrast to those exposed to NDL-PCBs, the larvae exposed to the DL-PCB126 and NDL-PCB118 had a response latency and rate similar to the control larvae.

The different startle response bends exhibit different kinematics, with SLCs exhibiting larger bend angles and faster angular velocities than LLCs (Burgess and Granato 2007). Thus, LLC and SLC kinematics were analyzed separately. PCB52-treated larvae had increased SLC bend angles (p > .0001) at two intermediate stimulus intensities (38 and 41 dB) while PCB126 larvae had increased SLC bend angles at the three highest stimulus intensities

(**Figure S7**). Furthermore, PCB153 (1000 nM) exposure resulted in an increased SLC bend angle at the highest stimulus intensity for those few larvae that exhibited an SLC (*n* = 26 of 138, 43 dB, $p < .0456$). LLC bend angle was significantly decreased across all stimulus intensities for PCB118. It is not clear how bend angle is associated with altered signaling and cellular function.

Cellular structures

The proper execution of the startle response relies on hair cells that sense the auditory stimulus, M-cells to integrate the signals, and motor neurons and musculature to execute the startle behavior. Morphological analysis showed that M-cells, motor neurons, and musculature all appeared unaffected by PCB153, but the hair cell innervating neurons appeared to be swollen (**Figure 3**). The L3 neuromast volume of control larvae was on average 569 μm^3 (*SD* = 125), whereas PCB153-exposed larvae (1000 nM) had significantly larger L3 neuromast volumes 848 μm^3 (*SD* = 185), $t(48.93) = 6.765$, $p < .0001$ (**Figure 3B**). However, the number of hair cells in L3 neuromasts (**Figure 3C**) and the intensity of FM1-43 dye internalized by hair cells (**Figure 3D**) remained unchanged in PCB153-treated larvae in comparison to the control.

The presence of M-cells is necessary for the SLC startle response. Staining with anti-3A10 confirmed the presence of M-cells in all PCB153-exposed larvae (21/21) (**Figure 4A**). We tested the functional responsiveness of the M-cells by applying electric field pulses to head-restrained larvae. This electrical stimulation bypasses the sensory system and directly activates the M-cell (Tabor et al. 2014). There was no difference detected in response time between control and 1000 nM PCB153-exposed larvae ($U = 907.5$, $p = .489$), demonstrating that the signal transmission from the M-cell to the motor neurons is not disrupted in PCR153-exposed fish (**Figure S8A**). The fraction responding also was similar in both the DMSO-treated (290/299) and the PCB153-treated (209/219) groups (GLM, $p = .427$; **Figure 4C, Figure S8B**). However, the C-bend evoked by the electrical stimulation was larger in PCB153-exposed larvae (*M* = 101.4, *SD* = 38.60) than in the control larvae (*M* = 83.12, *SD* =

24.23). An unpaired t-test with Welch-s correction indicated that this difference was statistically significant, $t(74.27) = 2.679$, $p = .0091$ (**Figure S8C**). This difference could indicate a PCB153-evoked functional alteration of the M-cell axon or motor neuron.

For rapid and effective axonal signal transmission, proper myelination of axons is key. We did not find PCB153 to reduce cells of the oligodendrocyte lineage in the spinal cord, ($t(36) = .553$, $p < .584$) nor any obvious differences in myelination itself (**Figure S9**).

Proper function and activation of the motor neurons is crucial for completion of the startle circuit, leading to muscle contractions and the characteristic swimming behaviors. The main caudal primary (CaP), middle primary (MiP), and rostral primary (RoP) motor neurons did not show any distinct structural differences between exposed and control larvae (**Figure S10**). The fast muscle fibers in the myotome were not found to be differentially striated in either treatment groups (**Figure S11**). No structural difference in the motor neurons or the myotome was apparent in PCB153-exposed larvae, suggesting that the increased bend angle does not originate from any overt structural differences in the motor neurons or muscle fibers.

Neuronal activity

The release of neurotransmitters into the synaptic cleft is a characteristic process in signal transmission. Both serotonergic and dopaminergic neuromodulators can affect startle latency (Jain et al. 2018), and evidence has been found that NDL-PCBs alter these neuromodulators in mammals (e.g. Castoldi et al. 2006; Enayah et al. 2018; Wigestrand et al. 2013). We observed that PCB153 (1000 nM) altered the levels of several neurotransmitters in 6 dpf zebrafish larvae (**Figure 5A**). Significantly increased level of GABA ($t(6) = 9.719$, $p < .001$), choline-chloride ($t(6) = 8.459$, $p < .001$), 3-methoxytyramine hydrochloride ($t(6) = 3.803$, $p = .009$), and L-valine ($t(6) = 3.134$, $p = .020$) were measured in PCB-exposed larvae in comparison to control larvae; while L-Glutamine was decreased in comparison to control larvae ($t(6) = 5.966$, $p < .001$).

To assess the interaction between PCB-exposure and changes in neuromodulatory activity, we pharmacologically manipulated the neurotransmitter levels using dopamine, serotonin, and GABA receptor agonists and antagonists. In control larvae, a 30 min exposure to dopamine precursor L-DOPA and D2-receptor agonist Quinpirole, as well as serotonin precursor 5-HTP, shifted the response to LLC, at multiple intensities tested ($p < .01$; **Figure 5C**). In contrast, the dopamine antagonist haloperidol exposure induced a shift to SLC in controls across all stimulus intensities ($p < .01$; **Figure 5C**). Haloperidol induced the same shift to SLC in PCB153-exposed larvae ($p < .001$), suggesting that the startle circuit is functional but repressed by PCB (**Figure 5C**). The response rate remained unchanged after exposure to neurotransmitter modulators except 5-HT, which caused an increase in response probability across all stimulus intensities in control larvae ($p < .01$); Quinpirole, which caused a decrease in response probability at the two lowest stimulus intensities in control larvae ($p < .01$); and Haloperidol, which caused an increase in response probability at 41 dB in PCB153-treated larvae ($p < .01$; **Figure S6**). It is noteworthy, that co-exposure to L-DOPA and PCB153 throughout development increased the response rate of PCB153-treated larvae significantly ($p < .01$), yet only induced a significant shift towards SLC at 38 dB ($p < .01$; **Figure S5C and S6C**).

In the fish brain, a distinct population of serotonergic neurons is found in the posterior tuberculum/hypothalamus, forming a prominent horseshoe-like pattern that is one of several brain regions where 5-HT is synthesized (Oikonomou et al. 2019). To assess whether the development of serotonergic cells in the brain of PCB153 larvae was affected, we performed immunohistochemistry using an antibody for 5-HT (**Figure S12**). The intensity of the fluorescent signal in the hypothalamus was not different, comparing PCB153 ($M = 4.70 \times 10^6$, $SD = 2.10 \times 10^6$) with the control ($M = 4.38 \times 10^6$, $SD = 8.1 \times 10^5$) group. This suggests that the serotonergic neurons in this region were not affected.

During specific behaviors or sensory experiences, only a small percentage of neurons are active. We analyzed the active neuronal cell populations in PCB153-treated and -untreated

larvae, focusing on the rostral hindbrain, where the M-cells are located, to assess whether there were changes in neural activity. We examined neuronal activity using the CaMPARI zebrafish line, which contains a protein that upon UV illumination permanently photoconverts from green to red fluorescence in cells with high calcium levels (Fosque et al. 2015). This genomic tool enabled us to look for active neuronal cell populations in larvae during normal swimming movement, and in larvae experiencing a vibroacoustic stimulated startle response, both in embryo medium at room temperature (24 °C), and at a colder temperature (4 °C). A higher red to green ratio (F_{red}/F_{green}) was measured comparing cold medium with room temperature medium: swimming control larvae in cold medium had a higher F_{red}/F_{green} ratio (M = 2.30, SD = 0.51) in comparison to swimming control larvae at RT (M = 0.96, SD = 0.17), confirming the potential of cold medium to elicit higher neuronal activity (**Figure S13**). However, this difference was diminished in PCB153-treated, yet still significant in trial 1: $F(1, 18) = 121$, $adj.\ p < .001$ and trial 2: $F(1, 32) = 65.2$, $adj.\ p = .041$. Importantly, the difference between swimming control and PCB153-treated larvae in cold medium was significant in both trial 1: $F(1, 18) = 121$, $adj.\ p = .028$ and trial 2 $F(1, 32) = 65.2$, $adj.\ p < .001$ (**Figure 5**). Similar differences in neuronal activity between control and PCB-153 treated larvae were measured for startling larvae during photoconversion (**Figure S13**).

Discussion

Despite most use ending decades ago, PCBs remain an important and persistent pollutant impacting both wildlife and humans. To date, mechanistic studies of neurodevelopmental effects of NDL-PCBs suggest two major targets: (1) alterations in neurotransmission, particularly involving dopamine and serotonin, and consequently disruptions to Ca^{2+} signal transduction (Campagna et al. 2011; Dervola et al. 2015; Enayah et al. 2018; Fonnum and Mariussen 2009; Langeveld et al. 2012), and (2) loss of outer hair cells (Crofton et al. 2000; Trnovec et al. 2010) or cochlear development (Goldey et al. 1995). However, such studies have not addressed how PCBs exert developmental neurobehavioral deficits, and thus we

do not know whether neurobehavioral disorders resulting from prenatal exposure originate in a structural effect in the auditory system, a neurotransmitter imbalance, or both. In this study we used the zebrafish startle response to comprehensively investigate the effects of different PCBs on neuron development and signal transmission and to assess effects at environmentally relevant concentrations for both humans and aquatic life. All NDL-PCBs delayed the acoustic startle response in zebrafish larvae, which coincided with axonal swelling and dysregulated GABA and dopamine metabolite levels. Co-exposures to the dopamine D2-receptor antagonist and GABA receptor modulator drug haloperidol, alleviated the delay in startle response.

The morphology of the neuronal cell body (perikarya) and neurite provides essential information on the developmental and physiological abnormalities in the neural circuits. We found that in PCB153-exposed larvae, the neurons that innervate the hair cells had an increased volume (**Figure 3**), indicating that PCB153 alters neuronal structure and hair cell function. Swelling of afferent terminals is associated with hearing deficits in both mammalian models (Puel et al. 1991) and zebrafish (Sebe et al. 2017). The increased volume may originate from increased numbers of bulged (swollen) afferent neurite termini or increased arborization (branching). For example, *tmie* mutant zebrafish, which are deaf with defective hair-cell function (Gleason et al. 2009), have more complex peripheral arbors in afferent axons and an increased number of neurites. In wildtype zebrafish, neurites with swollen axonal terminals are associated with hair cells of both polarities rather than just a single polarity, suggesting a dysregulation of selection in synaptic targets (Faucherre et al. 2010). At the sub-cellular level, neuronal swelling is due to increased cationic permeability in neurons, causing an osmotic imbalance that leads to water entry and cytotoxic edema (Rungta et al. 2015). While we examined a number of morphological features of the startle circuit anatomy (hair cell, afferent neurons, M-cell, oligodendrocyte lineage cells, myelination, motor neuron, muscle), only the volume of the neurons that innervate the hair cells showed a measurable deviation in PCB153-exposed larvae. We thus infer that the

548 enlargement of axon termini is contributing to the neurotoxic potential of NDL-PCBs – an
549 understudied target of PCB toxicity. A few studies associate NDL-PCB exposure with altered
550 dendritic arborization (Lein et al. 2007; Yang et al. 2009). Axonal swelling is a pathology
551 appearing in many neurodegenerative disease (Coleman 2005), and exposure to NDL-PCBs
552 may be a contributing factor in such diseases.

553 The startle response in fish and amphibians is a fundamental mechanism involved in
554 predator escape. Acoustic stimuli can trigger two distinct motor behaviors: a short-latency C-
555 bend (SLC**; Figure 2A**) initiated within 5-15 ms of the stimulus, or a long-latency C-bend
556 (LLC; **Figure 2A**), initiated within 15-100 ms (Burgess and Granato 2007). At the structural
557 level, laser-ablation of the M-cell abolishes SLC responses without affecting LLC responses
558 (Lacoste et al. 2015), suggesting that the LLC is a 'backup' response (Burgess and Granato
559 2007). The finding that NDL-PCB-exposed larvae predominantly exhibit LLC without loss of
560 M-cells (**Figure 4A**), suggests that the M-cells are receiving a delayed input, are not firing
561 properly, or that the signal propagation downstream of the M-cell is disrupted. To distinguish
562 these, we directly activated the M-cells by applying electrical stimulation to control larvae
563 with their heads restrained, and found that unlike auditory stimulation, PCB153-exposed fish
564 had latencies indistinguishable from the controls. Furthermore, direct stimulation of PCB153-
565 exposed larvae resulted in a normal response rate and response time, although the bend
566 angle was significantly increased. These results indicate a proper function of M-cells in NDL-
567 PCB-treated larvae. However, the changes in bend angles we observed during these
568 responses could indicate alterations downstream of the M-cells.

569 There is less known about the mechanisms leading to an aberrant turning angle. Since we
570 found no obvious structural impairment downstream of the M-cell (oligodendrocyte lineage
571 cells, myelination, motor neuron, musculature), we speculate that the increased bend angle
572 in electrically stimulated larvae exposed to PCB153 may be linked to a sub-cellular
573 disruption such as gap junctions. It is known that PCBs can alter gap junction function in

574 cells of many organs (Bager et al. 1997; Kang et al. 1996; Machala et al. 2003) including
575 NDL-PCB specific inhibition of gap junctional intercellular communication in neural crest cells
576 (Nyffeler et al. 2018) and neuronal stem cells (PCB153; (Kang et al. 2001)). Gap junctions
577 are intercellular channels formed by connexins (Cx). RNA sequencing of zebrafish larvae
578 exposed to PCB153 in a similar exposure regime (4-120 hpf) and concentration (10 μM)
579 significantly altered the expression of connexin genes cx28.9, cx42, and cx35b (Aluru et al.
580 2020). Cx35 is expressed on the Mauthner neuron lateral dendrites in zebrafish (Jain et al.
581 2018) and plays a crucial role in regulating spinal motor activity during fast motor behavior of
582 adult mosquitofish (Serrano-Velez et al. 2014). We thus propose that gap junction function
583 could be disrupted, which may be a future study direction using single-cell RNA sequencing
584 or genetically encoded optogenetics that has yet to be developed in a model organism (Dong
585 et al. 2018).

586 Neurotransmitters also play a key role in the startle response. A previous screening of more
587 than 1000 pharmacologically active compounds identified serotonergic and dopaminergic
588 modulators among the largest class of drugs that shift bias between SLC and LLC startle
589 behavior (Jain et al. 2018). Specifically, acute exposure to the D3R agonist (7OHD) shifted
590 the startle bias from LLC to SLC, while exposure to a D3R antagonist (or a 5-HT1AR
591 agonist) shifted bias toward LLC behavior (Jain et al. 2018). Our results extend these
592 findings, showing that 30 minutes exposure to L-DOPA or 5-HTP induces a shift from SLC to
593 LLC at higher stimulus intensities, as opposed to the D2R antagonist haloperidol, which
594 evoked a shift to a stronger SLC bias at all stimulus intensities (**Figure 5C**). NDL-PCBs are
595 thought to affect dopaminergic pathways (Mariussen and Fonnum 2001; Tanaka et al. 2018;
596 Wigestrand et al. 2013), which is partly supported by our measurements of catecholamines
597 and traces amines. Specifically, we found that the extracellular dopamine metabolite 3-
598 methoxytyramine hydrochloride and the inhibitory transmitter GABA were significantly
599 increased (**Figure 5A**). The interplay between dopamine and GABA receptors activity is
600 complex. In the mammalian system, dopamine is a direct-acting modulator of $GABA_A$Rs

(Hoerbelt et al. 2015). The simultaneous presence of a dopamine metabolite and GABA in PCB153-exposed zebrafish larvae may indicate that increased levels of GABA are a downstream effect of dysregulated dopamine activity. With both dopamine and GABA playing critical roles in motor activity, we hypothesize that PCB153 impairs dopaminergic neurotransmission and subsequently increases GABA levels, leading to the predominant LLC response. One of the most crucial regulators of synapse development and function mediating the GABAergic, dopaminergic, and serotonergic synaptic transmission is the brain derived neurotrophic factor (BDNF). PCB153 induced the expression of *bdnf* in zebrafish larvae (Aluru et al. 2020) suggesting BDNF as potential target for transcriptional regulation. Furthermore, we propose that GABA is involved in the swelling of the afferent terminals (**Figure 3**) as GABA activates Cl^- channels leading to an influx of Cl^- accompanied by H_2O (Cesetti et al. 2012; Rungta et al. 2015). The osmotic neuronal swelling alters neuronal activity. This study thus provides new evidence that GABA is involved in the neurobehavioral mode of action of higher chlorinated NDL-PCBs, as has been for lower chlorinated congeners (Fernandes et al. 2010).

An important finding of this study is that PCB153-exposed larvae can execute SLC when treated with haloperidol, a D2-antagonist that can increase dopamine turnover in acute exposure (Magnusson et al. 1987). There is a large body of evidence showing that NDL-PCBs, including PCB153, modulate dopaminergic neurotransmission by inhibiting the dopamine precursor enzyme tyrosine hydroxylase and dopamine synthesis itself, in both neural crest cells and adult laboratory animal models including non-human primates (Dervola et al. 2015; Enayah et al. 2018; Fonnum and Mariussen 2009; Seegal et al. 1990). In zebrafish larvae, PCB153 exposure during development elicited differential expression of nine genes related to the dopamine pathway, including tyrosine hydroxylase 2 (th2) (Aluru et al. 2020). Yet linking such effects to behavior is rare. Tanaka et al. (2018) suggested that the NDL-PCB dominant mixture Aroclor 1254 and BDE-47 functionally inhibited dopaminergic

neurons in early zebrafish embryos, as increased activity in 26 hpf embryos was inhibited by supplementation with L-tyrosine and L-DOPA (Tanaka et al. 2018).

The restoration of the delayed startle phenotype by haloperidol, together with the increased levels of a dopamine metabolite and GABA in PCB153-exposed larvae (**Figure 5A**), indicates that disruption of dopaminergic and GABAergic signaling between neurons of the auditory circuit is the dominant effect of PCB153-mediated aberrant motor behavior. These signaling processes are widely conserved across vertebrate species, and are important in human neurological diseases. For example, a recent study found that multiple gene mutations causing defective startle response in zebrafish were also associated with disorders of the locomotor system in humans (Meserve et al. 2020).

The localization of the PCB-induced disruption of dopaminergic signal transmission is likely downstream of the hair cells, potentially in the hindbrain. Although dopaminergic neurons innervate lateral line neuromasts, where D1R antagonist reduces the hair cell activity (Toro et al. 2015), we found no difference in the hair cell activity of PCB153-exposed larvae (**Figure 3D**). This is in contrast to the hindbrain, where neuronal activity was reduced in PCB153 exposed CaMPARI zebrafish larvae (**Figure 5**), indicating a reduced capacity for release or turnover of calcium. Intracellular Ca^{2+} signaling in neurons controls neurotransmitter secretion among many other cellular processes and thus may be indirectly involved in dopamine or GABA regulation. Some NDL-PCBs (PCB 95, 138) are known to inhibit voltage-gated calcium channels (Langeveld et al. 2012) contributing to interference with calcium homeostasis and consequently neurotransmission and synaptic plasticity (Brunelli et al. 2012; Campagna et al. 2011; Gafni et al. 2003; Ta et al. 2006).

The startle response to threatening stimuli is vital for survival. PCB153-exposed zebrafish larvae predominantly responded with a LLC, which not only delays the response, increasing the chance to be caught by a predator, but also usually does not displace the animal from its original location (**Figure 2A** and Jain et al., 2018). While survival of predator attack is likely

context-dependent and species-specific, escaping fast and away from a predator increases survival in the field (McCormick et al. 2018). This suggests that exposure to NDL-PCBs may alter selection pressure and thereby shift population structure. We have observed a significantly delayed startle response at concentrations as low as 10 nM (3.6 µg L^{-1}). PCBs are associated with sediments, where concentrations of PCB153 frequently reach multiple µg kg^{-1} (Lai et al. 2015). PCB concentrations in organisms may be even higher due to extensive bioconcentration (Killifish from New Bedford Harbor have 6.5 to 7 µg of PCB153 per g wet weight; Gräns et al. 2015). All NDL-PCBs tested in this study increased the startle latency. Thus, in the environment, where PCBs occur in mixtures of numerous congeners that likely have additive effects, the effect concentration is suggested to be lower than that of single congeners. Taken together, these results highlight the importance of the neurotoxic potential of NDL-PCBs in an ecological context.

In conclusion, the comprehensive approach presented here suggests that NDL-PCBs alter dopamine signaling, leading to an increase in GABA that ultimately results in swelling of axonal terminals in the auditory circuit. While the involvement of connexins remains speculative, our findings provide a foothold into the dopamine dysregulating potential of NDL-PCBs in sensory-motor processing in developing vertebrates, and link that to motor behavior. In a direct comparison, the present study demonstrates that the adverse behavioral effects are induced by all NDL-PCBs tested, but not by the classical DL-PCB126. Whether this is true for compounds that are structurally similar to NDL-PCBs, such as some PBDEs, is not known and will require further research. A key finding is that the effect of NDL-PCBs on the startle latency occurs at concentrations relevant for both environmental and human exposures, and therefore may contribute to the selection pressure in the environment and neurotoxicological disease in human. This study provides valuable clues for tackling health effects in humans and wildlife caused by environmental exposure.

CRediT authorship contribution statement

Nadja R. Brun: Conceptualization, Methodology, Formal analysis, Investigation, Writing - original draft, Writing - review & editing, Visualization, Funding acquisition. **Jennifer M. Panlilio:** Conceptualization, Methodology, Software, Formal analysis, Investigation, Writing - review & editing, Funding acquisition. **Kun Zhang:** Methodology, Investigation, Writing - review & editing, Funding acquisition. **Yanbin Zhao:** Methodology, Investigation, Writing - review & editing, Funding acquisition. **Evgeny Ivashkin:** Methodology, Investigation. **John J. Stegeman:** Conceptualization, Writing - review & editing, Funding acquisition. **Jared V. Goldstone:** Conceptualization, Writing - review & editing, Project administration.

Funding

This work was supported by the Swiss National Science Foundation P2EZP2_165200 (NRB), the Boston University Superfund Research Program NIH 5P42ES007381 (JJS and JVG), the Woods Hole Center for Oceans and Human Health (NIH: P01ES021923 and P01ES028938; NSF: OCE-1314642 and OCE-1840381) (NRB, JMP and JJS), and the National Natural Science Foundation of China 22006099 (KZ and YZ) and the Shanghai Pujiang Program 19PJ1404900 (KZ and YZ).

Acknowledgments

The authors would like to thank Neel Aluru for helpful discussion and providing the confocal microscope and Ed Levin and Mark Hahn for critically reading the manuscript and making valuable suggestions.

References

Almeida RG, Czopka T, Ffrench-Constant C, Lyons DA. 2011. Individual axons regulate the myelinating potential of single oligodendrocytes in vivo. Development 138:4443–50; doi:10.1242/dev.071001.

Aluru N, Krick KS, Mcdonald AM, Karchner SI. 2020. Developmental exposure to PCB153 (2,2′,4,4′,5,5′-hexachlorobiphenyl) alters circadian rhythms and the expression of clock

and metabolic genes. Toxicol Sci 173:41–52; doi:10.1093/toxsci/kfz217.

Bager Y, Lindebro MC, Martel P, Chaumontet C, Wärngård L. 1997. Altered function, localization and phosphorylation of gap junctions in rat liver epithelial, IAR 20, cells after treatment with PCBs or TCDD. Environ Toxicol Pharmacol 3:257–266; doi:10.1016/S1382-6689(97)00021-5.

Bates D, Mächler M, Bolker B, Walker S. 2015. Fitting Linear Mixed-Effects Models using lme4. J Stat Softw 67:1–48; doi:10.18637/jss.v067.i01.

Berger DF, Lombardo JP, Jeffers PM, Hunt AE, Bush B, Casey A, et al. 2001. Hyperactivity and impulsiveness in rats fed diets supplemented with either Aroclor 1248 or PCB-contaminated St. Lawrence river fish. Behav Brain Res 126:1–11; doi:10.1016/S0166-4328(01)00244-3.

Bergonzi R, Specchia C, Dinolfo M, Tomasi C, De Palma G, Frusca T, et al. 2009. Distribution of persistent organochlorine pollutants in maternal and foetal tissues: Data from an Italian polluted urban area. Chemosphere 76:747–754; doi:10.1016/j.chemosphere.2009.05.026.

Boix J, Cauli O, Felipo V. 2010. Developmental exposure to polychlorinated biphenyls 52, 138 or 180 affects differentially learning or motor coordination in adult rats. Mechanisms involved. Neuroscience 167:994–1003; doi:10.1016/j.neuroscience.2010.02.068.

Boucher O, Muckle G, Bastien CH. 2009. Prenatal exposure to polychlorinated biphenyls: A neuropsychologic analysis. Environ Health Perspect 117:7–16; doi:10.1289/ehp.11294.

Brunelli L, LLansola M, Felipo V, Campagna R, Airoldi L, De Paola M, et al. 2012. Insight into the neuroproteomics effects of the food-contaminant non-dioxin like polychlorinated biphenyls. J Proteomics 75:2417–2430; doi:10.1016/J.JPROT.2012.02.023.

Burgess HA, Granato M. 2007. Sensorimotor gating in larval zebrafish. J Neurosci 27:4984–4994; doi:10.1523/JNEUROSCI.0615-07.2007.

Campagna R, Brunelli L, Airoldi L, Fanelli R, Hakansson H, Heimeier RA, et al. 2011. Cerebellum Proteomics addressing the cognitive deficit of rats perinatally exposed to the food-relevant polychlorinated biphenyl 138. Toxicol Sci 123:170–179; doi:10.1093/toxsci/kfr156.

Castoldi AF, Blandini F, Randine G, Samuele A, Manzo L, Coccini T. 2006. Brain monoaminergic neurotransmission parameters in weanling rats after perinatal exposure to methylmercury and 2,2′,4,4′,5,5′-hexachlorobiphenyl (PCB153). Brain Res 1112:91–98; doi:10.1016/j.brainres.2006.07.022.

Cesetti T, Ciccolini F, Li Y. 2012. GABA not only a neurotransmitter: Osmotic regulation by GABA AR signaling. Front Cell Neurosci 6; doi:10.3389/fncel.2012.00003.

Chen Y-CJ, Guo Y-L, Hsu C-C, Rogan WJ. 1992. Cognitive development of Yu-Cheng ('Oil Disease') children prenatally exposed to heat-degraded PCBs. JAMA J Am Med Assoc 268:3213; doi:10.1001/jama.1992.03490220057028.

Coccini T, Roda E, Castoldi AF, Poli D, Goldoni M, Vettori MV, et al. 2011. Developmental exposure to methylmercury and 2,2′,4,4′,5,5′-hexachlorobiphenyl (PCB153) affects

744 cerebral dopamine D1-like and D2-like receptors of weanling and pubertal rats. Arch
745 Toxicol 85:1281–1294; doi:10.1007/s00204-011-0660-y.

746 Coleman M. 2005. Axon degeneration mechanisms: Commonality amid diversity. Nat Rev
747 Neurosci 6:889–898; doi:10.1038/nrn1788.

748 Crofton KM, Ding D-L, Padich R, Taylor M, Henderson D. 2000. Hearing loss following
749 exposure during development to polychlorinated biphenyls: A cochlear site of action.
750 Hear Res 144:196–204; doi:10.1016/S0378-5955(00)00062-9.

751 Dervola KSN, Johansen EB, Walaas SI, Fonnum F. 2015. Gender-dependent and genotype-
752 sensitive monoaminergic changes induced by polychlorinated biphenyl 153 in the rat
753 brain. Neurotoxicology 50:38–45; doi:10.1016/J.NEURO.2015.07.004.

754 Dong A, Liu S, Li Y. 2018. Gap junctions in the nervous system: Probing functional
755 connections using new imaging approaches. Front Cell Neurosci 12:1–9;
756 doi:10.3389/fncel.2018.00320.

757 Enayah SH, Vanle BC, Fuortes LJ, Doorn JA, Ludewig G. 2018. PCB95 and PCB153
758 change dopamine levels and turn-over in PC12 cells. Toxicology 394:93–101;
759 doi:10.1016/j.tox.2017.12.003.

760 Ennaceur S, Gandoura N, Driss MR. 2008. Distribution of polychlorinated biphenyls and
761 organochlorine pesticides in human breast milk from various locations in Tunisia: Levels
762 of contamination, influencing factors, and infant risk assessment. Environ Res 108:86–
763 93; doi:10.1016/J.ENVRES.2008.05.005.

764 Faucherre A, Baudoin JP, Pujol-Martí J, López-Schier H. 2010. Multispectral four-
765 dimensional imaging reveals that evoked activity modulates peripheral arborization and
766 the selection of plane-polarized targets by sensory neurons. Development 137:1635–
767 1643; doi:10.1242/dev.047316.

768 Fernandes ECA, Hendriks HS, Van Kleef RGDM, Van Den Berg M, Westerink RHS. 2010.
769 Potentiation of the human GABAA receptor as a novel mode of action of lower-
770 chlorinated non-dioxin-like PCBs. Environ Sci Technol 44:2864–2869;
771 doi:10.1021/es902321a.

772 Fonnum F, Mariussen E. 2009. Mechanisms involved in the neurotoxic effects of
773 environmental toxicants such as polychlorinated biphenyls and brominated flame
774 retardants. J Neurochem 111:1327–1347; doi:10.1111/j.1471-4159.2009.06427.x.

775 Fosque BF, Sun Y, Dana H, Yang C, Ohyama T, Tadross MR, et al. 2015. Labeling of active
776 neural circuits in vivo with designed calcium integrators. Science 347: 755–760.

777 Gafni J, Wong PW, Pessah IN. 2003. Non-coplanar 2,2',3,5',6-pentachlorobiphenyl (PCB 95)
778 amplifies ionotropic glutamate receptor signaling in embryonic cerebellar granule
779 neurons by a mechanism involving ryanodine receptors. Toxicol Sci 77:72–82;
780 doi:10.1093/toxsci/kfh004.

781 Gleason MR, Nagiel A, Jamet S, Vologodskaia M, López-Schier H, Hudspeth AJ. 2009. The
782 transmembrane inner ear (Tmie) protein is essential for normal hearing and balance in
783 the zebrafish. Proc Natl Acad Sci U S A 106:21347–21352;
784 doi:10.1073/pnas.0911632106.

785 Goldey ES, Kehn LS, Lau C, Rehnberg GL, Crofton KM. 1995. Developmental exposure to
786 polychlorinated biphenyls (Aroclor 1254) reduces circulating thyroid hormone
787 concentrations and causes hearing deficits in rats. Toxicol Appl Pharmacol 135:77–88;
788 doi:10.1006/TAAP.1995.1210.

789 Grandjean P, Landrigan PJ. 2014. Neurobehavioural effects of developmental toxicity.
790 Lancet Neurol 13:330–338; doi:10.1016/S1474-4422(13)70278-3.

791 Gräns J, Wassmur B, Fernández-Santoscoy M, Zanette J, Woodin BR, Karchner SI, et al.
792 2015. Regulation of pregnane-X-receptor, CYP3A and P-glycoprotein genes in the
793 PCB-resistant killifish (Fundulus heteroclitus) population from New Bedford Harbor.
794 Aquat Toxicol 159:198–207; doi:10.1016/j.aquatox.2014.12.010.

795 Herbstman JB, Sjödin A, Apelberg BJ, Witter FR, Patterson DG, Halden RU, et al. 2007.
796 Determinants of prenatal exposure to polychlorinated biphenyls (PCBs) and
797 polybrominated diphenyl ethers (PBDEs) in an urban population. Environ Health
798 Perspect 115:1794–1800; doi:10.1289/ehp.10333.

799 Hoerbelt P, Lindsley TA, Fleck MW. 2015. Dopamine directly modulates GABAA receptors. J
800 Neurosci 35:3525–3536; doi:10.1523/JNEUROSCI.4390-14.2015.

801 Howe K, Clark MD, Torroja CF, Torrance J, Berthelot C, Muffato M, et al. 2013. The
802 zebrafish reference genome sequence and its relationship to the human genome.
803 Nature 496:498–503; doi:10.1038/nature12111.

804 Hudspeth A. 1985. The cellular basis of hearing: the biophysics of hair cells. Science
805 230:745–752; doi:10.1126/science.7414321.

806 Inoue D, Wittbrodt J. 2011. One for all-a highly efficient and versatile method for fluorescent
807 immunostaining in fish embryos. PLoS One 6:1–7; doi:10.1371/journal.pone.0019713.

808 Jain RA, Wolman MA, Marsden KC, Nelson JC, Shoenhard H, Echeverry FA, et al. 2018. A
809 forward genetic screen in zebrafish identifies the G-protein-coupled receptor CaSR as a
810 modulator of sensorimotor decision making. Curr Biol 28:1357-1369.e5;
811 doi:10.1016/j.cub.2018.03.025.

812 Johansen EB, Fonnum F, Lausund PL, Walaas SI, Bærland NE, Wøien G, et al. 2014.
813 Behavioral changes following PCB 153 exposure in the Spontaneously Hypertensive rat
814 - an animal model of Attention-Deficit/Hyperactivity disorder. Behav Brain Funct 10:1–
815 19; doi:10.1186/1744-9081-10-1.

816 Jusko TA, Sisto R, Iosif A-M, Moleti A, Wimmerová S, Lancz K, et al. 2014. Prenatal and
817 postnatal serum PCB concentrations and cochlear function in children at 45 months of
818 age. Environ Health Perspect 122:1246–1252; doi:10.1289/ehp.1307473.

819 Kang K-S, Park J-E, Ryu D-Y, Lee Y-S. 2001. Effects and neuro-toxic mechanisms of
820 2,2',4,4',5,5'-hexachlorobiphenyl and endosulfan in neuronal stem cells. J Vet Med Sci
821 63:1183–1190; doi:10.1292/jvms.63.1183.

822 Kang KS, Wilson MR, Hayashi T, Chang CC, Trosko JE. 1996. Inhibition of gap junctional
823 intercellular communication in normal human breast epithelial cells after treatment with
824 pesticides, PCBs, and PBBs, alone or in mixtures. Environ Health Perspect 104:192–
825 200; doi:10.1289/ehp.96104192.

826 Kimmel CB. 1993. Patterning the brain of the zebrafish embryo. Annu Rev Neurosci 16:707–
827 732; doi:10.1146/annurev.ne.16.030193.003423.

828 Lacoste AMB, Schoppik D, Robson DN, Haesemeyer M, Portugues R, Li JM, et al. 2015. A
829 convergent and essential interneuron pathway for mauthner-cell-mediated escapes.
830 Curr Biol 25:1526–1534; doi:10.1016/j.cub.2015.04.025.

831 Lai Z, Li X, Li H, Zhao L, Zeng Y, Wang C, et al. 2015. Residual distribution and risk
832 assessment of polychlorinated biphenyls in surface sediments of the Pearl River Delta,
833 South China. Bull Environ Contam Toxicol 95:37–44; doi:10.1007/s00128-015-1563-z.

834 Lancz K, Hertz-Picciotto I, Jusko TA, Murínová Ľ, Wimmerová S, Šovčíková E, et al. 2015a.
835 Duration of breastfeeding and serum PCB 153 concentrations in children. Environ Res
836 136:35–39; doi:10.1016/j.envres.2014.09.036.

837 Lancz K, Palkovičováa L, Patayová H, Drobná B, Wimmerová S, Šovčíková E, et al. 2015b.
838 Ratio of cord to maternal serum PCB concentrations in relation to their congener-
839 specific physicochemical properties. Int J Hyg Env Heal 218:91–98;
840 doi:doi:10.1016/j.ijheh.2014.08.003.

841 Landrigan PJ, Fuller R, Acosta NJR, Adeyi O, Arnold R, Basu N, et al. 2018. The Lancet
842 Commission on pollution and health. Lancet 391:462–512; doi:10.1016/S0140-
843 6736(17)32345-0.

844 Langeveld WT, Meijer M, Westerink RHS. 2012. Differential effects of 20 non-dioxin-like
845 PCBs on basal and depolarization-evoked intracellular calcium levels in PC12 cells.
846 Toxicol Sci 126:487–496; doi:10.1093/toxsci/kfr346.

847 Lein PJ, Yang D, Bachstetter AD, Tilson HA, Harry GJ, Mervis RF, et al. 2007. Ontogenetic
848 alterations in molecular and structural correlates of dendritic growth after developmental
849 exposure to polychlorinated biphenyls. Environ Health Perspect 115:556–563;
850 doi:10.1289/ehp.9773.

851 Lilienthal H, Heikkinen P, Andersson PL, van der Ven LTM, Viluksela M. 2011. Auditory
852 effects of developmental exposure to purity-controlled polychlorinated biphenyls
853 (PCB52 and PCB180) in rats. Toxicol Sci 122:100–111; doi:10.1093/toxsci/kfr077.

854 Lilienthal H, Korkalainen M, Andersson PL, Viluksela M. 2015. Developmental exposure to
855 purity-controlled polychlorinated biphenyl congeners (PCB74 and PCB95) in rats:
856 Effects on brainstem auditory evoked potentials and catalepsy. Toxicology 327:22–31;
857 doi:10.1016/J.TOX.2014.11.004.

858 Liu YC, Hale ME. 2017. Local spinal cord circuits and bilateral mauthner cell activity function
859 together to drive alternative startle behaviors. Curr Biol 27:697–704;
860 doi:10.1016/j.cub.2017.01.019.

861 Machala M, Bláha L, Vondráček J, Trosko JE, Scott J, Upham BL. 2003. Inhibition of gap
862 junctional intercellular communication by noncoplanar polychlorinated biphenyls:
863 Inhibitory potencies and screening for potential Mode(s) of Action. Toxicol Sci 76:187–
864 195; doi:10.1093/TOXSCI.

865 Magnusson O, Mohringe B, Thorell G, Lake-Bakaar DM. 1987. Effects of the dopamine D2
866 selective receptor antagonist remoxipride on dopamine turnover in the rat brain after

867 acute and repeated administration. Pharmacol Toxicol 60:368–373; doi:10.1111/j.1600-
868 0773.1987.tb01529.x.

869 Mariussen E, Fonnum F. 2001. The effect of polychlorinated biphenyls on the high affinity
870 uptake of the neurotransmitters, dopamine, serotonin, glutamate and GABA, into rat
871 brain synaptosomes. Toxicology 159:11–21; doi:10.1016/S0300-483X(00)00374-7.

872 Maximino C, Herculano AM. 2010. A review of monoaminergic neuropsychopharmacology in
873 zebrafish. Zebrafish 7:359–378; doi:10.1089/zeb.2010.0669.

874 McCormick MI, Fakan E, Allan BJM. 2018. Behavioural measures determine survivorship
875 within the hierarchy of whole-organism phenotypic traits. Funct Ecol 32:958–969;
876 doi:10.1111/1365-2435.13033.

877 Medan V, Preuss T. 2014. The Mauthner-cell circuit of fish as a model system for startle
878 plasticity. J Physiol Paris 108:129–140; doi:10.1016/j.jphysparis.2014.07.006.

879 Meserve JH, Nelson JC, Marsden KC, Hsu J, Echeverry FA, Jain A, et al. 2020. A forward
880 genetic screen identifies Dolk as a regulator of startle magnitude through the potassium
881 channel subunit Kv1.1. bioRxiv.

882 Meyers JR, MacDonald RB, Duggan A, Lenzi D, Standaert DG, Corwin JT, et al. 2003.
883 Lighting up the senses: FM1-43 loading of sensory cells through nonselective ion
884 channels. J Neurosci 23:4054–65; doi:10.1523/JNEUROSCI.23-10-04054.2003.

885 Nakayama H. 2004. Common sensory inputs and differential excitability of segmentally
886 homologous reticulospinal neurons in the hindbrain. J Neurosci 24:3199–3209;
887 doi:10.1523/JNEUROSCI.4419-03.2004.

888 Nyffeler J, Chovancova P, Dolde X, Holzer AK, Purvanov V, Kindinger I, et al. 2018. A
889 structure–activity relationship linking non-planar PCBs to functional deficits of neural
890 crest cells: new roles for connexins. Arch Toxicol 92:1225–1247; doi:10.1007/s00204-
891 017-2125-4.

892 Oikonomou G, Altermatt M, Zhang R wei, Coughlin GM, Montz C, Gradinaru V, et al. 2019.
893 The serotonergic raphe promote sleep in zebrafish and mice. Neuron 103:686-701.e8;
894 doi:10.1016/j.neuron.2019.05.038.

895 Panlilio JM, Aluru N, Hahn ME. 2020. Developmental neurotoxicity of the harmful algal
896 bloom toxin domoic acid: Cellular and molecular mechanisms underlying altered
897 behavior in the zebrafish Model. Environ Health Perspect 128:117002;
898 doi:10.1289/EHP6652.

899 Panlilio JM, Jones IT, Salanga MC, Aluru N, Hahn ME. 2021. Developmental exposure to
900 domoic acid disrupts startle response behavior and circuitry. bioRxiv;
901 doi:10.1101/2021.01.08.425996.

902 Park H-C, Shin J, Roberts RK, Appel B. 2007. An olig2 reporter gene marks oligodendrocyte
903 precursors in the postembryonic spinal cord of zebrafish. Dev Dyn 236:3402–3407;
904 doi:10.1002/dvdy.21365.

905 Poon E, Bandara SB, Allen JB, Sadowski RN, Schantz SL. 2015. Developmental PCB
906 exposure increases susceptibility to audiogenic seizures in adulthood. Neurotoxicology

907 46:117–124; doi:10.1016/j.neuro.2014.12.007.

908 Puel JL, Pujol R, Ladrech S, Eybalin M. 1991. α-Amino-3-hydroxy-5-methyl-4-isoxazole
909 propionic acid electrophysiological and neurotoxic effects in the guinea-pig cochlea.
910 Neuroscience 45:63–72; doi:10.1016/0306-4522(91)90103-U.

911 Pujol-Martí J, López-Schier H. 2013. Developmental and architectural principles of the
912 lateral-line neural map. Front Neural Circuits 7:47; doi:10.3389/fncir.2013.00047.

913 Ranasinghe P, Thorn RJ, Seto R, Creton R, Bridges WC, Chapman SC, et al. 2019.
914 Embryonic exposure to 2,2′,3,5′,6-pentachlorobiphenyl (PCB-95) causes developmental
915 malformations in zebrafish. Environ Toxicol Chem 39:162–170; doi:10.1002/etc.4587.

916 Ribas-Fitó N, Sala M, Kogevinas M, Sunyer J. 2001. Polychlorinated biphenyls (PCBs) and
917 neurological development in children: A systematic review. J Epidemiol Community
918 Health 55:537–546; doi:10.1136/jech.55.8.537.

919 Rice D, Barone S. 2000. Critical periods of vulnerability for the developing nervous system:
920 Evidence from humans and animal models. Environ Health Perspect 108:511–533;
921 doi:10.2307/3454543.

922 Roberts A. 2000. Early functional organization of spinal neurons in developing lower
923 vertebrates. Brain Res Bull 53:585–593; doi:10.1016/S0361-9230(00)00392-0.

924 Rungta RL, Choi HB, Tyson JR, Malik A, Dissing-Olesen L, Lin PJC, et al. 2015. The cellular
925 mechanisms of neuronal swelling underlying cytotoxic edema. Cell 161:610–621;
926 doi:10.1016/j.cell.2015.03.029.

927 Schindelin J, Arganda-Carreras I, Frise E, Kaynig V, Longair M, Pietzsch T, et al. 2012. Fiji:
928 An open-source platform for biological-image analysis. Nat Methods 9:676–682;
929 doi:10.1038/nmeth.2019.

930 Sebe JY, Cho S, Sheets L, Rutherford MA, von Gersdorff H, Raible DW. 2017. Ca^{2+}-
931 permeable AMPARs mediate glutamatergic transmission and excitotoxic damage at the
932 hair cell ribbon synapse. J Neurosci 37:6162–6175; doi:10.1523/jneurosci.3644-
933 16.2017.

934 Seegal RF, Bush B, Shain W. 1990. Lightly chlorinated ortho-substituted PCB congeners
935 decrease dopamine in nonhuman primate brain and in tissue culture. Toxicol Appl
936 Pharmacol 106: 136–44.

937 Serrano-Velez JL, Rodriguez-Alvarado M, Torres-Vazquez II, Fraser SE, Yasumura T,
938 Vanderpool KG, et al. 2014. Abundance of gap junctions at glutamatergic mixed
939 synapses in adult Mosquitofish spinal cord neurons. Front Neural Circuits 8:66;
940 doi:10.3389/fncir.2014.00066.

941 Shin J, Park H-C, Topczewska JM, Mawdsley DJ, Appel B. 2003. Neural cell fate analysis in
942 zebrafish using <i>olig2<i> BAC transgenics. Methods Cell Sci 25:7–14;
943 doi:10.1023/B:MICS.0000006847.09037.3a.

944 Smith NL, Kimelman D. 2019. *Establishing the body plan: The first 24 hours of zebrafish*
945 *development*. Elsevier.

946 Stenberg M, Hamers T, Machala M, Fonnum F, Stenius U, Lauy AA, et al. 2011. Multivariate
947 toxicity profiles and QSAR modeling of non-dioxin-like PCBs - An investigation of in vitro
948 screening data from ultra-pure congeners. Chemosphere 85:1423–1429;
949 doi:10.1016/j.chemosphere.2011.08.019.

950 Stewart AM, Braubach O, Spitsbergen J, Gerlai R, Kalueff A V. 2014. Zebrafish models for
951 translational neuroscience research: From tank to bedside. Trends Neurosci 37:264–
952 278; doi:10.1016/j.tins.2014.02.011.

953 Ta TA, Feng W, Molinski TF, Pessah IN. 2006. Hydroxylated xestospongins block inositol-
954 1,4,5-trisphosphate-induced Ca^{2+} release and sensitize Ca^{2+}-induced Ca^{2+} release
955 mediated by ryanodine receptors. Mol Pharmacol 69:532–538;
956 doi:10.1124/mol.105.019125.used.

957 Tabor KM, Bergeron SA, Horstick EJ, Jordan DC, Aho V, Porkka-Heiskanen T, et al. 2014.
958 Direct activation of the Mauthner cell by electric field pulses drives ultrarapid escape
959 responses. J Neurophysiol 112:834–844; doi:10.1152/jn.00228.2014.

960 Takada N, Kucenas S, Appel B. 2010. Sox10 is necessary for oligodendrocyte survival
961 following axon wrapping. Glia 58:996–1006; doi:10.1002/glia.20981.

962 Tanaka Y, Fujiwara M, Shindo A, Yin G, Kitazawa T, Teraoka H. 2018. Aroclor 1254 and
963 BDE-47 inhibit dopaminergic function manifesting as changes in locomotion behaviors
964 in zebrafish embryos. Chemosphere 193:1207–1215;
965 doi:10.1016/j.chemosphere.2017.11.138.

966 Toro C, Trapani JG, Pacentine I, Maeda R, Sheets L, Mo W, et al. 2015. Dopamine
967 modulates the activity of sensory hair cells. J Neurosci 35:16494–16503;
968 doi:10.1523/JNEUROSCI.1691-15.2015.

969 Trnovec T, Šovčíková E, Pavlovčinová G, Jakubíková J, Jusko TA, Husťák M, et al. 2010.
970 Serum PCB concentrations and cochlear function in 12-year-old children. Environ Sci
971 Technol 44:2884–2889; doi:10.1021/es901918h.

972 Troconis EL, Ordoobadi AJ, Sommers TF, Aziz-Bose R, Carter AR, Trapani JG. 2017.
973 Intensity-dependent timing and precision of startle response latency in larval zebrafish.
974 J Physiol 595:265–282; doi:10.1113/JP272466.

975 Tropepe V, Sive HL. 2003. Can zebrafish be used as a model to study the
976 neurodevelopmental causes of autism? Genes, Brain Behav 2:268–281;
977 doi:10.1034/j.1601-183X.2003.00038.x.

978 Vettori MV, Goldoni M, Caglieri A, Poli D, Folesani G, Ceccatelli S, et al. 2006. Antagonistic
979 effects of methyl-mercury and PCB153 on PC12 cells after a combined and
980 simultaneous exposure. Food Chem Toxicol 44:1505–1512;
981 doi:10.1016/j.fct.2006.04.009.

982 Voesenek CJ, Muijres FT, Van Leeuwen JL. 2018. Biomechanics of swimming in developing
983 larval fish. J Exp Biol 221; doi:10.1242/jeb.149583.

984 Walkowiak J, Wiener J-A, Fastabend A, Heinzow B, Krämer U, Schmidt E, et al. 2001.
985 Environmental exposure to polychlorinated biphenyls and quality of the home
986 environment: effects on psychodevelopment in early childhood. Lancet 358:1602–1607;

doi:10.1016/S0140-6736(01)06654-5.

Wigestrand MB, Stenberg M, Walaas SI, Fonnum F, Andersson PL. 2013. Non-dioxin-like PCBs inhibit [3H]WIN-35,428 binding to the dopamine transporter: A structure–activity relationship study. Neurotoxicology 39:18–24; doi:10.1016/J.NEURO.2013.07.005.

Wolman MAA, Jain RAA, Marsden KCC, Bell H, Skinner J, Hayer KEE, et al. 2015. A genome-wide screen identifies PAPP-AA-mediated IGFR signaling as a novel regulator of habituation learning. Neuron 85:1200–1211; doi:10.1016/j.neuron.2015.02.025.

Yang D, Kim KH, Phimister A, Bachstetter AD, Ward TR, Stackman RW, et al. 2009. Developmental exposure to polychlorinated biphenyls interferes with experience-dependent dendritic plasticity and ryanodine receptor expression in weanling rats. Environ Health Perspect 117:426–435; doi:10.1289/ehp.11771.

Zhao Y, Liang J, Meng H, Yin Y, Zhen H, Zheng X, et al. 2020. Rare earth elements lanthanum and praseodymium adversely affect neural and cardiovascular development in zebrafish (Danio rerio). Environ Sci Technol; doi:10.1021/acs.est.0c06632.

Figures

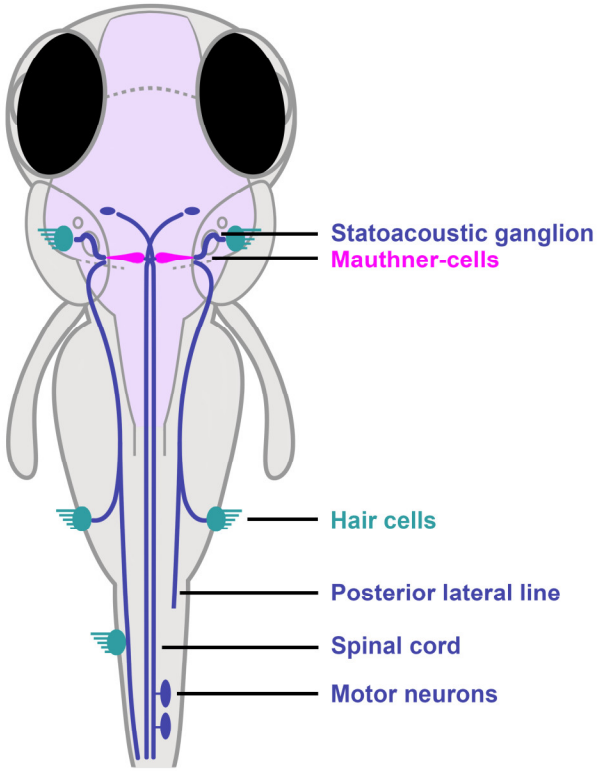

Figure 1. Startle response circuit in zebrafish. The proper execution of the startle response relies on hair cells to sense the auditory stimulus, Mauthner-cells to integrate the signals, and motor neurons and musculature to execute the startle behavior.

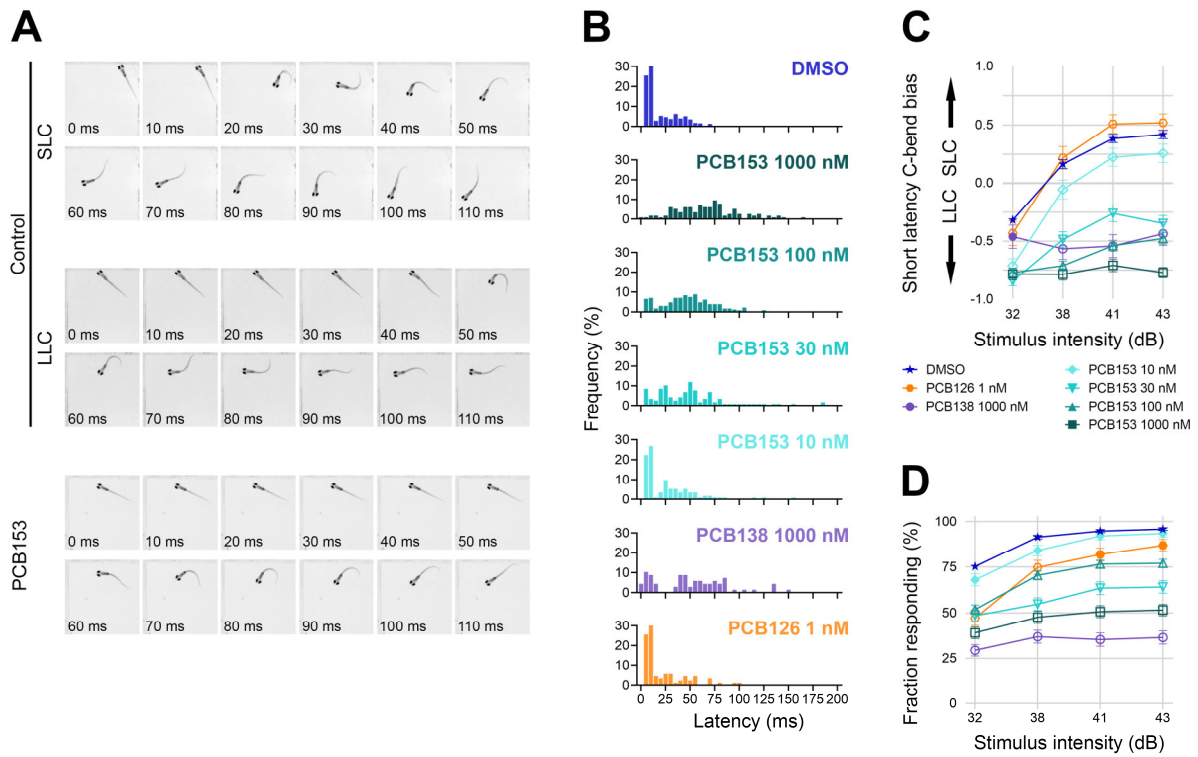

Figure 2. Effect of PCBs on startle response in 6 dpf zebrafish. (A) Representative short-latency C-bend (SLC) and long-latency C-bend (LLC) startle response of a control zebrafish larva at 6 dpf in comparison to a typical response of a PCB153 treated larva. (B) Vibro-acoustic startle latency at highest stimulus intensity (43 dB) in vehicle control (*n* = 479), NDL-PCB153 1000 nM (*n* = 179), NDL-PCB153 100 nM (*n* = 253), NDL-PCB153 30 nM (*n* = 152), NDL-PCB153 10 nM (*n* = 119), NDL-PCB138 (*n* = 139), and DL-PCB126 (n = 97) exposed larvae. (C) Bias of SLC and LLC and (D) response rate of different exposure groups at different vibro-acoustic intensities. Values are presented as mean ± SEM. All data points are biologically independent replicates from at least three independent experiments. Significant differences to DMSO controls ($p < 0.01$) are indicated by open symbols.

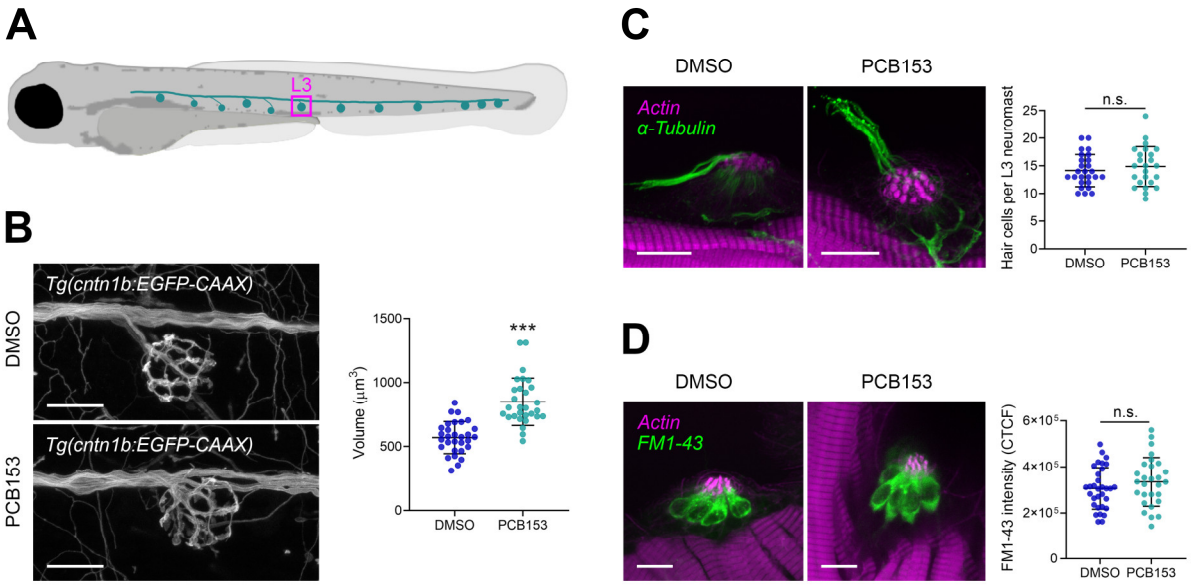

1017 **Figure 3. Effect of PCB153 on morphology and function of lateral line hair cells and**
1018 **innervating neurons.** (**A**) Diagram indicating L3 neuromast. (**B**) Hair cell innervating neurons
1019 at neuromast L3 shown using *Tg(cntn1b:EGFP-CAAX)*. Volume of hair cell innervating
1020 neurons of DMSO (*n* = 30) and PCB153 (*n* = 29) treated larvae. Scale bar = 20 µm. (**C**) Whole-
1021 mount immune staining of kinocilia and hair cell innervating neurons (anti-acetylated tubulin
1022 antibody; green) and counterstain of stereocilia bundles and muscle tissue (actin; magenta) of
1023 DMSO (*n* = 26) and PCB153 (*n* = 24) treated larvae. The hair cell number was determined
1024 based on the number of kinocilia. Scale bar = 10 µm (**D**) Uptake of FM-143 dye as indication
1025 of functional hair cells of DMSO (*n* = 32) and PCB153 (*n* = 28) treated larvae. Scale bar = 10
1026 µm. All data points are biologically independent replicates from at three independent
1027 experiments. Asterisks indicate significant differences to controls (***p < 0.0001).

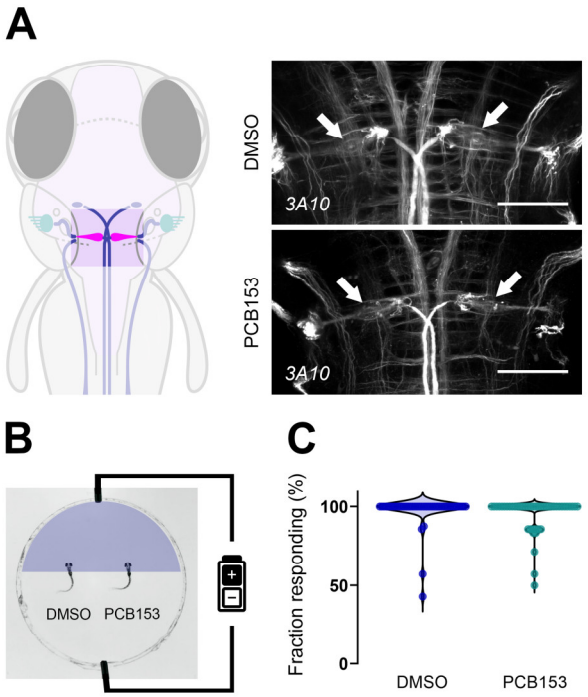

Figure 4. Effect of PCB153 on morphology and function of the Mauthner-cells. (**A**) Diagram indicating localization of Mauthner-cells in the hindbrain. Brain tissue immunostaining with anti-neurofilament 3A10 antibody labeling reticulospinal neurons in control and PCB153 treated larvae at 6 dpf (ventral view). Mauthner (arrow) cells were present in all brain tissues (control: *n* = 23, PCB153: *n* = 21). Scale bar = 50 µm. (**B**) Diagram of electrical stimulation performed to assess the functionality of Mauthner-cells. (**C**) Percentage of responders to electrical stimulation. All data points are biologically independent replicates from at least three independent experiments.

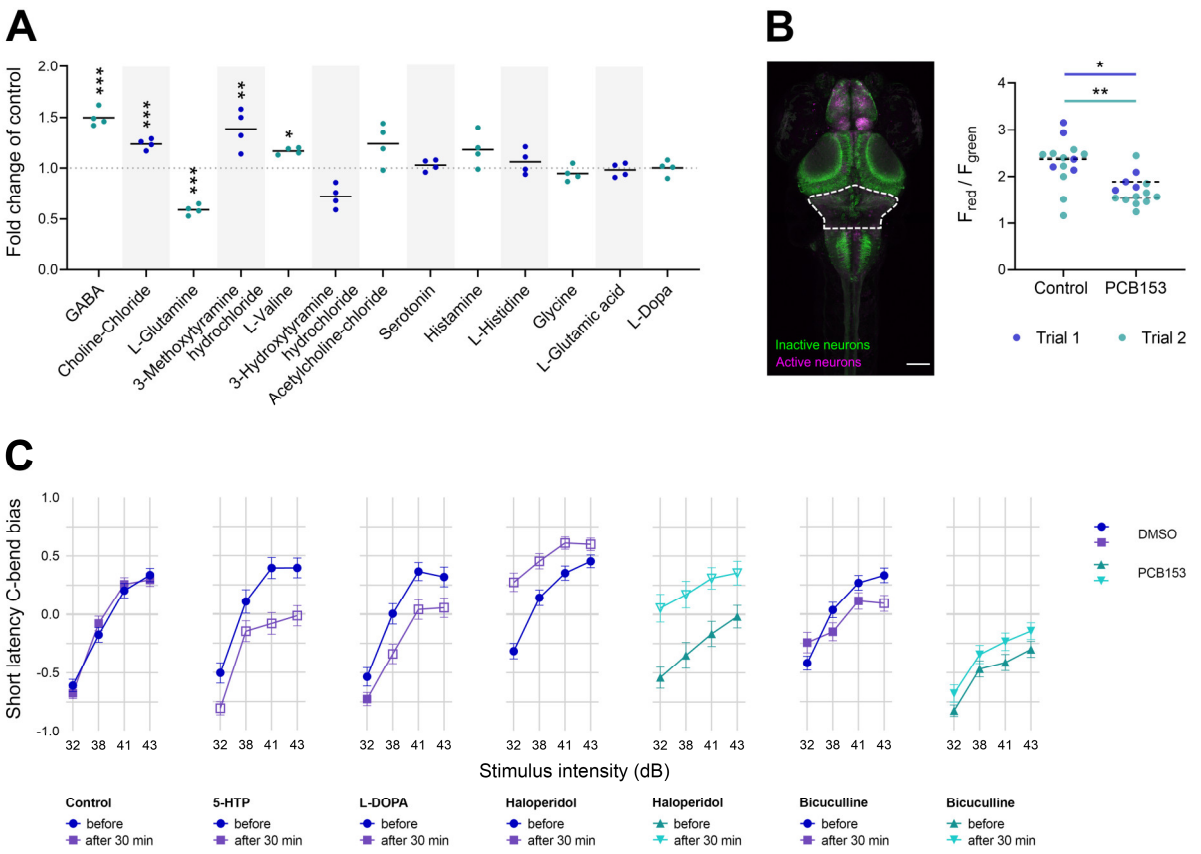

Figure 5. Involvement of neurotransmitters in startle latency. (**A**) Neurotransmitter levels in 6 dpf larvae exposed to 1000 nM PCB153 in comparison to control (*n* = 4). (**B**) Representative maximum intensity z-projection from confocal stack after photoconversions of freely swimming 6 dpf CaMPARI larvae. Scale bar = 100 µm. Ratio of red to green fluorescence intensity in the rostral hindbrain (indicated by dashed line in image) in DMSO (*n* = 14) and 1000 nM PCB153 (*n* = 14) exposed startling larvae in 4 ˚C (cold) medium. Dashed lines indicate median per trial. Two independent experiments. Asterisks indicate significant differences to controls (*p < 0.05, **p < 0.01, and ***p < 0.001). (**C**) Startle bias shift induced by 30-minute exposure to serotonin, dopamine, and GABA neurotransmitter modulators in 6 dpf control and 100 nM PCB153 exposed larvae. Control (*n* = 138-172), 5-HTP (*n* = 67-80), L-DOPA (*n* = 76-94), Haloperidol (Control *n* = 123-162, PCB153 *n* = 37-61), and Bicuculline (Control *n* = 90-162, PCB153 *n* = 83-137). All data points are biologically independent replicates from at least three independent experiments. Significant differences to respective controls (*p* < 0.01) are indicated by open symbols.